Journal of Thermal Science Vol.30, No.1 (2021) 149–164

**https://doi.org/10.1007/s11630-020-1291-5** **Article ID: 1003-2169(2021)01-0149-16**

# Performance Improvement of Single Screw Compressor by Meshing Clearance Adjustment Used in Refrigeration System

**LU Yuanwei[1,2*], LIU Shanwei[1,2], WU Yuting[1,2], LEI Biao[1,2], ZHI Ruiping[1,2], WEN Qiangyu[1,2], MA Chongfang[1,2]**

1. Key Laboratory of Enhanced Heat Transfer and Energy Conservation, Ministry of Education, College of Environmental and Energy Engineering, Beijing University of Technology, Beijing 100124, China
2. Key Laboratory of Heat Transfer and Energy Conversion, Beijing Municipality, College of Environmental and Energy Engineering, Beijing University of Technology, Beijing 100124, China



**Abstract:** The single screw compressor (SSC) is widely used in air compression and refrigeration systems due to its many advantages. The meshing clearance between the screw groove and gate rotor teeth flank has a significant influence on the compressor performance. In this paper, mathematical calculation models describing the internal working process of the SSC are established in order to evaluate the thermal dynamic characteristics of the compressor under varying meshing clearance heights. The refrigerating capacity, volume efficiency and adiabatic efficiency of the SSC are calculated and discussed. Three prototypes, with different meshing clearance heights, were manufactured to study the internal influence mechanisms. The theoretical model was verified using experimental data and the calculation results strongly agreed with the experimental results. Results demonstrate that comparisons of volume efficiency and adiabatic efficiency between the measured and calculated results exhibited deviations of 3.64%–7.98% and 5.92%–9.4%, respectively. Based on the models, analysis under varying meshing clearance heights and working conditions was performed. Taking into account working performance, actual manufacturing conditions and manufacturing cost limitations, a meshing clearance height range from 0.01 mm to 0.08 mm is suggested. This study can provide important theoretical data and experimental support for the design, manufacturing and optimization of single screw compressors.

**Keywords: single screw compressor, leakage, performance improvement, meshing clearance height, refrigeration**

## 1. Introduction

Both the academic community and industrial engineers are placing an increasing amount of attention on the development of high performance compressors [1]. Screw compressors are mainly divided into twin-screw compressors and single-screw compressors (SSC), and have been widely used in air compression, refrigeration, liquefied natural gas systems and heat pumps [2, 3]. Compared to twin-screw compressors, the geometry of SSC varies widely, resulting in significant variations in their operating characteristics and thermodynamic properties. For example, the twin-screw compressors have less wearing parts, can be operated for a long time,

Received: May 07, 2019 AE: ZHANG Hongwu Corresponding author: LU Yuanwei E-mail: luyuanwei@bjut.edu.cn

**Nomenclature**

**Variables**

| | |
|---|---|
| $c_f$ | speed of fluid/m·s$^{-1}$ |
| $d_e$ | equivalent diameter/m |
| $E$ | energy/J |
| $g$ | acceleration of gravity/m·s$^{-2}$ |
| $h$ | specific enthalpy/J·kg$^{-1}$ |
| $I$ | current/A |
| $k$ | heat convection coefficient/W·m$^{-2}$·K$^{-1}$ |
| $m$ | mass/kg |
| $\dot{m}$ | mass flow rate/kg·s$^{-1}$ |
| $P$ | power loss of motor/W |
| $p$ | pressure/Pa |
| $Pr$ | Prandtl number |
| $Q$ | heat transfer quantity/J |
| $R$ | harmonic resistance/Ω |
| $S$ | area/m$^2$ |
| $T$ | temperature/°C |
| $U$ | internal energy/J |
| $u$ | specific internal energy/J·kg$^{-1}$ |
| $V$ | volume/m$^3$ |
| $v$ | specific volume/m$^3$·kg$^{-1}$ |
| $W$ | work/J |
| $w$ | rotation angle speed/rad·s$^{-1}$ |
| $x$ | ratio of gas in the gas-oil mixture |
| $z$ | height/m |

**Greeks**

| | |
|---|---|
| $\alpha$ | void fraction |
| $\theta$ | rotation angle/rad |
| $\lambda$ | heat conductivity |
| $\xi$ | local loss coefficient |
| $\rho$ | working fluid density/kg·m$^{-3}$ |

**Subscripts**

| | |
|---|---|
| cu | copper |
| cv | control volume |
| d | outlet |
| f | friction |
| fe | iron |
| g | gas |
| i | in |
| in | fluid enter the control volume |
| l | oil |
| lg | leakage gas |
| lo | leakage oil |
| o | out |
| out | fluid leave the control volume |
| v | volume |
| w | wall |

use advanced technology, and are associated with low processing costs. However, the system force is unbalanced and the bearing is easily damaged. The SSC was first presented by Frenchman Zimmern and Patel in the 1960s [4]. Compared with other types of compressors [5], the SSC has many advantages, such as super low noise, a strong force balance, a simple structure, and a large single stage pressure ratio. However, the gate rotor of the SSC is easily worn, thus the gate rotor needs to be replaced regularly. The SSC can generally be divided into four categories: PC, CC, PP and CP. C represents the cylindrical screw and P represents the plate. The CP type is currently the most common SSC form. It has a meshing pair which consists of a screw and two symmetrically arranged gate rotor plates, while the meshing pair is the core working part during compression [6]. The compression chamber is composed of the screw groove, the profile surfaces of the gate rotor teeth and the internal wall of the shell. The volume of the compressor changes with the rotation of the screw and the gate rotors.

In order for the SSC to operate efficiently, an effective seal must be formed between the screw and the gate rotors and between the rotor and the shell. The length of the clearances that exhibit a leakage in the working fluid path will vary with the angle of the screw rotor, thus the working performance of the compressor changes during the compression process. Although it is clear that an increase of clearance in screw machines deteriorates efficiency, the effect of different meshing clearance heights on the performance of the SSC remains to be clearly understood. Moreover, the reduction in clearance rapidly increases the processing cost. For example, the manufacturing cost of a tool that processes the screw and gate rotor may reach thousands of dollars, and if the machining accuracy is doubled, it may increase the manufacturing cost of the tool by up to several times or more. Therefore, for the structural characteristics of SSC, it is important to establish a reasonable clearance range to ensure the performance of the compressor while at the same time controlling the manufacturing cost within a reasonable range. In addition, for the semi-hermetic refrigeration compressor, the dissipation heat generated by the motor is also a key factor that may influence the performance of the compressor. Consequently, the influence of different meshing clearance heights is of great engineering and economic significance.

At present, extensive research has been performed on

the working process of the SSC through theoretical and experimental methods. For the meshing process between the screw groove and gate rotor teeth, studies have focused on the structure and different configuration of the meshing pair. The original structure of the meshing pair is denoted as the straight line envelope meshing pair, invented by Zimmern in the 1960s, who also developed the column envelope meshing pair in the 1970s [7]. Huang et al. [8] developed an approach for the optimization of the gate rotor profile based on the column envelope meshing pair. More specifically, the lubrication states in clearance between the groove flanks and the teeth flanks were improved after optimization. In recent years, a new multi-column envelope meshing pair was created by Wu et al. [9] so as to enhance the wear resistance of the meshing pair. Based on this multi-column envelope, the geometrical model of the leakage path in the compressor was established by Wang et al. [10], reducing the leakage rate.

Li et al. [11] developed a numerical model to study the hydrodynamic lubrication properties of different meshing pair profiles based on water-flooded single screw compressors. In particular, research on the meshing pair aims to reduce the meshing clearance height value and the leakage rate of the working fluid, so as to improve the performance of the compressor. The screw compressor combines thermodynamics and flow processes, both of which are dependent on screw compressor geometry. Early research established a series of differential equations based on the law of conservation of mass and energy so as to analysis the compressor process. Thus, the pressure and temperature of the working fluid in the working chamber can be determined [12]. This was strongly supported in the literature, early examples of which are Fujiwara et al. 1974 [13], Fukazawa et al. 1980 [14], and Sangfors 1984 [15], for twin screw compressors. Based on the working characteristics of the SSC, the inventor Zimmern [16] studied the design and operating characteristics of the compressor in 1970s and established the basic design parameters including materials, the transmission ratio and clearance values. Because the performance and the reliability of this type of machine is affected by the lubrication and sealing, the oil injection working process has been the focus of some literature [17, 18]. Yang et al. [19] evaluated the wet compression in a mechanical vapor recompression system using the SSC based on water injection. It was found that the performance of the system significantly improved. Wang et al. [20, 21] applied a theoretical model under various load conditions in order to study the capacity control mechanism, and observed the optimization of the liquid injection process of the compressor. Zhao et al. [22] analyzed the heat transfer of the SSC under oil atomization based on a fuzzy random wavelet finite element method, and was able to determine the optimal atomization technology.

Most of the aforementioned studies focus on the profile of the meshing pair, leakage, lubrication and working process based on, for example, oil injection or water injection. The influence mechanism of meshing clearance variations on the performance of the compressor are yet to be considered. In this paper, a theoretical model considering many factors, such as the motor of the compressor, leakages, heat transfer and lubricating oil, is established to analyze the working characteristics of the SSC under different meshing clearances and working conditions. The influence of the motor dissipation heat and friction loss on the physical properties of the working medium is established and the variation law of thermal and physical parameters, such as pressure, temperature and mass in the working chamber with the screw rotation angle, are obtained. The volume efficiency and adiabatic efficiency under different meshing clearances are then analyzed and compared using these validated models. In order to verify the applicability of the theoretical calculation results, three prototype compressors with different meshing clearance heights of 0.05, 0.10 and 0.15 mm, are manufactured. The compressors are subsequently tested on the experimental system according to the gas loop method. The results can provide important theoretical data and experimental support for the design, manufacturing and optimization of single screw compressors. Finally, a suitable meshing clearance height range under the working conditions that can easily be applied by engineers and designers is provided.

## 2. Theoretical Calculation of the Single Screw Compressor

Fig. 1 shows the structure of the semi-hermetic SSC. The SSC comprises two main components: one screw and two symmetrically collocated planar gate rotors. The compression chamber is formed by the screw groove surface, the inner wall of the shell and the profile surface of the gate rotor teeth. The rotating power originates from the motor, and the volume of the working chamber changes with the screw rotation angle. The ratio of the number of teeth to the number of screw grooves is generally 11:6, and there are 12 compression chambers working at the same time. Before the working medium enters the compression chamber, the motor will cool down using the working fluid and the pressure of the working medium is reduced. Taking four grooves as an example, the whole working process can be divided into four phases: the suction in groove 1, the sealing in groove 2, the compression in groove 3 and the discharge in groove 4, as shown in Fig. 1. The compression process

will continue until the discharge port is connected to the working chamber. For the SSC, there are many factors, such as heat transfer, friction, geometric structure, leakage and operating conditions, that will affect the working performance.

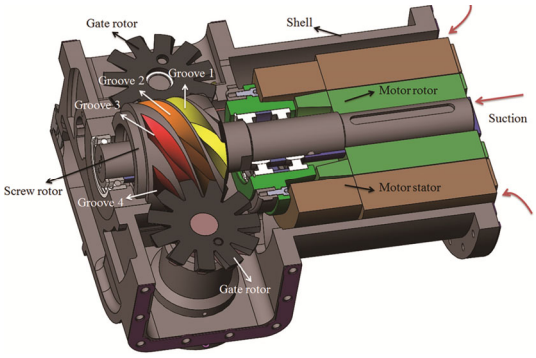


**Fig. 1** Schematic diagram of working process of the single screw compressor

In order to simplify the process, the following assumptions have been made to establish the mathematic model:

(1) In the control volume, the temperature and pressure distribution are uniform. The state parameters of the working fluid change periodically with the rotation angle.

(2) The state of the gas-oil mixture is homogeneous and the oil is treated as an incompressible fluid.

(3) The influences of the body forces of the working fluids are negligible.

### 2.1 Governing equation

In order to facilitate the analysis, one screw groove was selected as the control volume, as shown in Fig. 2.

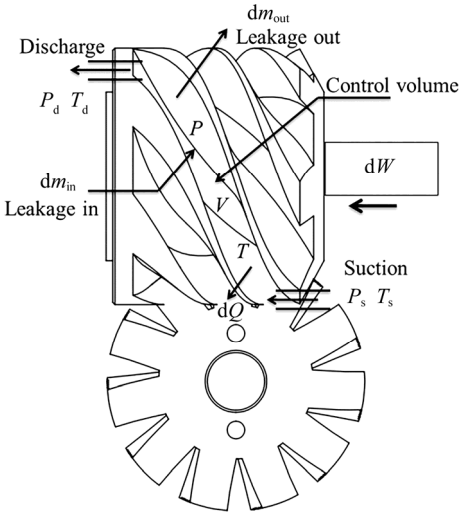


**Fig. 2** The control volume

According to the mass balance principle, the mass of the working fluid is given by:

$$\frac{\mathrm{d}\dot{m}}{\mathrm{d}\theta_1}=\sum\frac{\mathrm{d}\dot{m}_{\mathrm{in}}}{\mathrm{d}\theta_1}-\sum\frac{\mathrm{d}\dot{m}_{\mathrm{out}}}{\mathrm{d}\theta_1} \tag{1}$$

where $\theta_1$ is the screw rotation angle; $\dot{m}$ is the mass flow rate in the compression chamber; $\dot{m}_{\mathrm{in}}$ is the suction and leakage-in flow rate of the working fluid, and $\dot{m}_{\mathrm{out}}$ is the discharge and leakage-out flow rate of the working fluid. The parameters $\dot{m}_{\mathrm{in}}$ and $\dot{m}_{\mathrm{out}}$ can be calculated according to the leakage model in the following sections.

The energy conservation law for the control volume of the SSC can be expressed as follows:

$$\begin{aligned}\frac{\mathrm{d}E_{\mathrm{cv}}}{\mathrm{d}\theta_1}=&\sum\frac{\mathrm{d}\dot{m}_{\mathrm{in}}}{\mathrm{d}\theta_1}\left(h_{\mathrm{in}}+\frac{1}{2}c_{\mathrm{fin}}+gz_{\mathrm{in}}\right)\\&-\sum\frac{\mathrm{d}\dot{m}_{\mathrm{out}}}{\mathrm{d}\theta_1}\left(h_{\mathrm{out}}+\frac{1}{2}c_{\mathrm{out}}+gz_{\mathrm{out}}\right)\\&-\frac{\mathrm{d}Q}{\mathrm{d}\theta_1}+\frac{\mathrm{d}W}{\mathrm{d}\theta_1}\end{aligned} \tag{2}$$

If the potential and kinetic energy of the flow are ignored, the following equation can be obtained:

$$\frac{\mathrm{d}\left(\dot{m}u\right)_{\mathrm{cv}}}{\mathrm{d}\theta_1}=\sum\frac{\mathrm{d}\dot{m}_{\mathrm{in}}}{\mathrm{d}\theta_1}h_{\mathrm{in}}-\sum\frac{\mathrm{d}\dot{m}_{\mathrm{out}}}{\mathrm{d}\theta_1}h_{\mathrm{out}}-\frac{\mathrm{d}Q}{\mathrm{d}\theta_1}+\frac{\mathrm{d}W}{\mathrm{d}\theta_1} \tag{3}$$

From the basic thermodynamic equations, we can obtain the state parameters of the working fluid in the control volume (e.g. pressure, temperature and specific volume) as follows [15]:

$$\begin{aligned}&\frac{1}{v}\left[\left(\frac{\partial h}{\partial v}\right)_T-\frac{\left(\frac{\partial h}{\partial T}\right)_v\left(\frac{\partial p}{\partial v}\right)_T}{\left(\frac{\partial p}{\partial T}\right)_v}\right]\frac{\mathrm{d}v}{\mathrm{d}\theta}\\&\frac{\mathrm{d}p}{\mathrm{d}\theta_1}=\frac{-\frac{1}{V}\left[\sum\frac{\mathrm{d}\dot{m}_{\mathrm{in}}}{\mathrm{d}\theta_1}\left(h_{\mathrm{in}}-h\right)-\frac{\mathrm{d}Q}{\mathrm{d}\theta_1}\right]}{1-\frac{1}{v}\frac{\left(\frac{\partial h}{\partial T}\right)_v}{\left(\frac{\partial p}{\partial T}\right)_v}}\\&\left[\frac{1}{v}\left(\frac{\partial h}{\partial v}\right)_T-\left(\frac{\partial p}{\partial v}\right)_T\right]\frac{\mathrm{d}v}{\mathrm{d}\theta_1}\end{aligned} \tag{4}$$

$$\frac{\mathrm{d}T}{\mathrm{d}\theta_1}=\frac{-\frac{1}{V_{\mathrm{c}}}\left[\sum\frac{\mathrm{d}\dot{m}_{\mathrm{in}}}{\mathrm{d}\theta_1}\left(h_{\mathrm{in}}-h\right)-\frac{\mathrm{d}Q}{\mathrm{d}\theta_1}\right]}{\left(\frac{\partial p}{\partial T}\right)_v-\frac{1}{v}\left(\frac{\partial h}{\partial T}\right)_v} \tag{5}$$

$$\frac{\mathrm{d}v}{\mathrm{d}\theta_1}=\frac{1}{\dot{m}}\frac{\mathrm{d}V}{\mathrm{d}\theta_1}-\frac{V}{\dot{m}^2}\frac{\mathrm{d}\dot{m}}{\mathrm{d}\theta_1} \tag{6}$$

where $p$ is the volumetric element pressure; $T$ is the volumetric element temperature; $V$ is the volume element; $v$ is the specific volume; $\mathrm{d}W$ is the compression work; $\mathrm{d}Q$

is the heat transfer capacity, and $h$ and $u$ are the enthalpy and energy of the working fluid, respectively.

### 2.2 Leakage model

In the SSC, the geometrical structure of the leakage paths has a large influence on the performance of the compressor. Thus, based on the geometry of a SSC, nine leakage paths were summarized as shown in Fig. 3. $L_1$ is the clearance between the top of the gate rotor teeth and the bottom of the screw groove. Here, the length of $L_1$ will change with screw angle changes. $L_2$ is the clearance between the front surface of the gate rotor teeth flank and the screw groove. $L_4$ is the clearance between the rear surface of the gate rotor teeth flank and the screw groove. $L_3$ and $L_5$ are the blowholes enclosed by the screw groove, gate rotor teeth flank, and the case. $L_6$ is the gap between the shell and the surface of the gate rotor teeth. $L_7$ and $L_8$ are the clearances between the inner surface of the case and the front and rear edge of the screw groove. $L_9$ is the clearance between the inner surface of the case and the discharge edge of the working chamber.

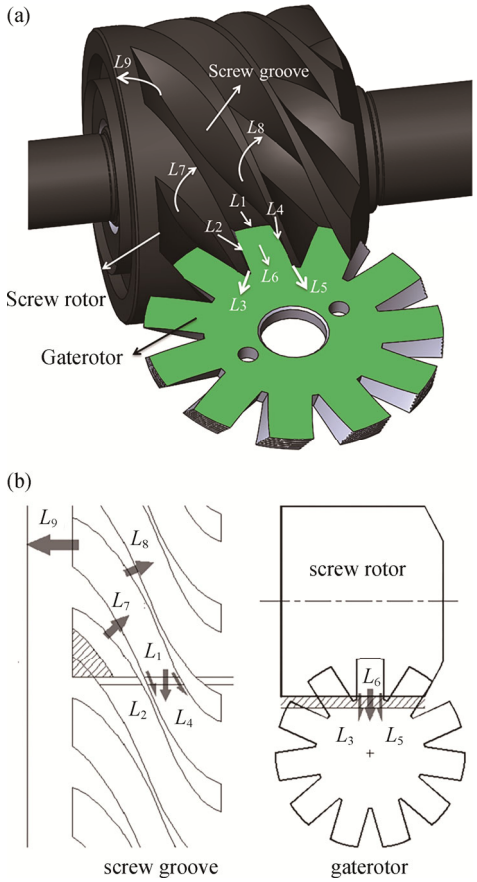


**Fig. 3** Leakage paths of the single screw compressor

Because of the lubricating oil, the working fluid in the compression chamber can be treated as a two-phase gas-oil mixture. The leakage flow rate through the nine leakage paths of the SSC can be obtained according to two-phase flow law [23]. It should be noted that the leakage rates of the working fluid are also depended on the curve shape of the gap walls. The geometrical description of the gaps and the equations of the nine leakage paths can be found in a previous study on single screw expanders [24]. Although the working processes of the single screw compressor and the single screw expanders are different, the geometrical structures of their leakage paths are the same.

The leakage mass flow rate of the working fluid can be calculated as follows:

$$\begin{cases} \dfrac{\mathrm{d}\dot{m}_{\mathrm{lg}}}{\mathrm{d}\theta} = C_{\mathrm{l}}\alpha\sum_{i=1}^{9} S_i\rho_{\mathrm{g}}c_{\mathrm{g}} \\ \dfrac{\mathrm{d}\dot{m}_{\mathrm{lo}}}{\mathrm{d}\theta} = C_{\mathrm{l}}(1-\alpha)\sum_{i=1}^{9} S_i\rho_{\mathrm{o}}c_{\mathrm{g}} / f \\ c_{\mathrm{g}} = \sqrt{2(h_{\mathrm{l}}-h_2)} \end{cases} \tag{7}$$

The slip factor $f$ and the void fraction $\alpha$ can be given by:

$$\begin{cases} f = 0.4 + 0.6\sqrt{\dfrac{\rho_l}{\rho_g} + 0.4\dfrac{1}{x-1}}\sqrt{1+0.4\dfrac{1}{x-1}} \\ \alpha = \dfrac{1}{1+f\dfrac{1}{x-1}\dfrac{\rho_g}{\rho_l}} \end{cases} \tag{8}$$

where, $\dot{m}_{\mathrm{lg}}$ is the leakage mass flow rate of the gas; $\dot{m}_{\mathrm{lo}}$ is the leakage mass flow rate of the lubricating oil, and $C_{\mathrm{l}}$ is the flow coefficient, which is set as 0.65 in this paper. We take the value of $C_{\mathrm{l}}$ from the literature [25, 26] based on the study of twin-screw compressors and expanders due to their similar geometrical structures for the leakage paths. $S_i$ is the area of the leakage path; $c_{\mathrm{g}}$ is the velocity of gas, and $\rho_{\mathrm{g}}$ and $\rho_{\mathrm{l}}$ are the density of the gas and oil, respectively. $x$ is the ratio of the gas in the oil-gas mixture; $f$ is the slip factor; $h_{\mathrm{l}}$ is the enthalpy of the high pressure end, and $h_2$ is the enthalpy in the low pressure chambers.

### 2.3 Heat transfer model

The heat transfer between the gas and the boundary of the working chambers can be described using the following equation [27]:

$$\frac{\mathrm{d}Q}{\mathrm{d}\theta_{\mathrm{l}}} = \frac{kS_{\mathrm{w}}\left(T-T_{\mathrm{w}}\right)}{w} \tag{9}$$

Moreover, the heat exchange between the gas and lubricating oil can be obtained as follows:

$$\frac{\mathrm{d}Q_{\mathrm{oil}}}{\mathrm{d}\theta_{\mathrm{l}}} = \frac{kS_{\mathrm{l}}\left(T_{\mathrm{l}}-T\right)}{w} \tag{10}$$

where $w$ is the angular speed of the screw; $k$ is the

coefficient of heat convection; $T$ is the working fluid temperature, and $T_w$ and $T_l$ are the temperature of the control volume wall and oil, respectively. $S_w$ is the heat exchange area; $S_l$ is the heat exchange area of the oil film, and $S_w$ and $S_l$ are basic geometrical parameters in the SSC that can be calculated according to [28].

The coefficient $k$ can be obtained by the following equation:

$$k = 0.023\frac{\lambda}{d_e}\left(\frac{\rho_g c_g d_e}{u_g}\right)Pr^n \tag{11}$$

where $\lambda$ is the heat conductivity of the gas; $d_e$ is the equivalent diameter of the working chamber; $u_g$ is the dynamic viscosity of the gas, and $c_g$ is the characteristic velocity for the $Re$ number of the working fluid. Here, the value of $n$ is 0.4 when the working fluid is heated, and 0.3 otherwise.

### 2.4 Friction power loss

The friction loss mainly denotes leakage power loss and viscosity power loss. For the calculation of the leakage flow rate, the leakage power loss was considered as a thermodynamic model [29]. According to Newton's friction law, the viscosity power loss can be expressed as follows [27]:

$$W_f = \sum_{i=1}^{9}\int_0^{b_i}\tau_f c_f L_i \mathrm{d}x \tag{12}$$

In addition, the shear stress of the fluid can be obtained as follows:

$$\tau_f = \mu\frac{\mathrm{d}c_f}{\mathrm{d}y} \tag{13}$$

where $\mu$ is the dynamic viscosity of the working fluid; $b_i$ is the width of the $i_{th}$ leakage path; $L_i$ is the length of the $i_{th}$ leakage path, and $c_f$ is the velocity of fluid in the gap.

### 2.5 Motor working process model

For the semi-hermetic SSC, the power is supplied by the motor and most of the motor dissipation heat is absorbed by the working fluid. Thus, the temperature of the working fluid will increase before the working fluid flows into the working chamber. In addition, the pressure will also decrease when the working fluid travels through the motor channels. Both factors will have a great influence on the state parameters of the suction working fluids and the thermodynamic performance. Moreover, the dynamic characteristics of the working fluid in the compressor will also be affected. Within the motor section, such internal flow problems will be solved with the aid of the Bernoulli equation as follows [30]:

$$\frac{p_i}{\rho g} + \alpha\frac{{c_{fi}}^2}{2g} + z_i = \frac{p_o}{\rho g} + \alpha\frac{{c_{fo}}^2}{2g} + z_o + h_\xi + h_f \tag{14}$$

$$h_\xi = \xi\frac{{c_f}^2}{2g} \tag{15}$$

$$h_f = f\left(\frac{l}{d_h}\right)\frac{{c_f}^2}{2g} \tag{16}$$

where $\alpha$ is a correction factor of the kinetic energy; $p_i$ and $p_o$ are the inlet and outlet pressure of the motor, respectively; $c_{fi}$ and $c_{fo}$ are the inlet and outlet velocity of the motor, respectively; $\rho$ is the density of the working fluid; $h_\xi$ is the local resistance loss; $h_f$ is the loss due to frictional resistance; $\xi$ is the local loss coefficient; $f$ is the Darcy friction factor; $l$ is the channel length of the motor; and $d_h$ is the equivalent diameter of channel.

Based on the motor design theory, the dissipation power generated by the motor in the energy conversion process mainly includes the copper, iron and the stray loss, and can be calculated according to [31]. As shown in Fig. 4, the power loss can be derived using the equivalent circuit method for the fixed frequency motor, where, $c$ is the correction factor; $R_1$ is the phase resistance of stator winding; $R_2$ is the rotor resistance; $R_m$ is the excitation resistance; $s$ is the slip ratio of the motor; $I_1$ is the stator current; $I_2$ is the rotor current; $I_m$ is the field current; $x_1$ is the stator leakage reactance; $x_2$ is the rotor leakage reactance; and $x_m$ is the excitation reactance.

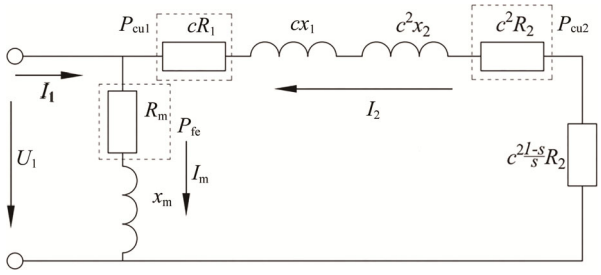


**Fig. 4** Type $\Gamma$ equivalent circuit

The copper loss of the motor can be calculated by the following equation:

$$P_{cu} = m\left(I_1^2 R_1 + I_2^2 R_2\right) \tag{17}$$

Moreover, the iron loss of the motor can be derived as follows:

$$P_{fe} = mI_m^2 R_m \tag{18}$$

The bearing friction loss can be expressed as follows:

$$P_f = 0.15\frac{F}{d}u\times 10^{-5} \tag{19}$$

while the total energy loss can be obtained by the follow equation:

$$P_T = p_{cu} + p_{fe} + p_f + p_s \tag{20}$$

where $m$ is the phase number of the motor; $F$ is the

bearing load; $d$ is the diameter of the bearing ball; $u$ is the velocity of the bearing ball, and $p_s$ is the stray loss.

The increase in temperature of the suction working fluid caused by the motor can be calculated by the following equation:

$$\Delta T_g = \frac{P_T}{\dot{m}_g C_g} \tag{21}$$

where, $\dot{m}_g$ is the mass flow rate of the working fluid; $C_g$ is the specific heat capacity of the working fluid, and $\Delta T_g$ is the temperature difference of the working fluid.

By analyzing the mathematic model that describes the working process of the motor, the pressure drop and the temperature rise of the working fluid occurring through the motor can be obtained.

### 2.6 Calculation method of the model

Based on the basic governing equations above, a mathematic model that is able to describe the thermodynamic working process of the compressor was established. Fig. 5 presents the flowchart of the method. First, the geometry parameters of the single screw compressor and operating conditions shown in Table 1 should be taken as the initial parameters required to establish the mathematic model. The governing Eqs. (14)–(21) can then be solved to calculate the pressure drop and temperature rise of the working fluid. The parameters are initialized with the assumption of no leakage and isentropic compression of the working process. Based on models that take into account leakages, heat transfer and lubricating oil, the Runge-Kutta method was used to determine the numerical solution of the equations and the thermodynamic transient state parameters of the working process, including $P(\theta_1)$, $T(\theta_1)$, and $m(\theta_1)$. When the absolute value of $\xi$, the difference in pressure between the last two calculations, reaches the precision requirements, we obtain the required state parameters and the thermophysical parameters of the working fluid can then be derived using the Martin-Hou Equation [32].

### 2.7 Performance parameters

The volumetric efficiency is an important evaluation criterion for compressor performance used to evaluate the leakage effect. The volumetric efficiency can be obtained by:

$$\eta_v = \frac{\dot{m}_{real}}{\dot{m}_{th}} \tag{22}$$

The theoretical mass flow rate $\dot{m}_{th}$ can be expressed as follows:

$$\dot{m}_{th} = 2Nz_1V_{in}\rho_{in} \tag{23}$$

where $N$ is the rotate speed of the screw rotor; $z_1$ is the number of rotor grooves (taken as 6 in this paper); $\rho_{in}$ is the density of the working medium, and $V_{in}$ is the theoretical volume element. The real mass flow rate $\dot{m}_{real}$ can be measured using a flow meter in the test system, or calculated in the mathematical model by:

$$\dot{m}_{real} = \dot{m}_{th} - \dot{m}_{lg} \tag{24}$$

where $\dot{m}_{lg}$ is the leakage mass flow rate of the gas, and can be calculated according to the leakage model.

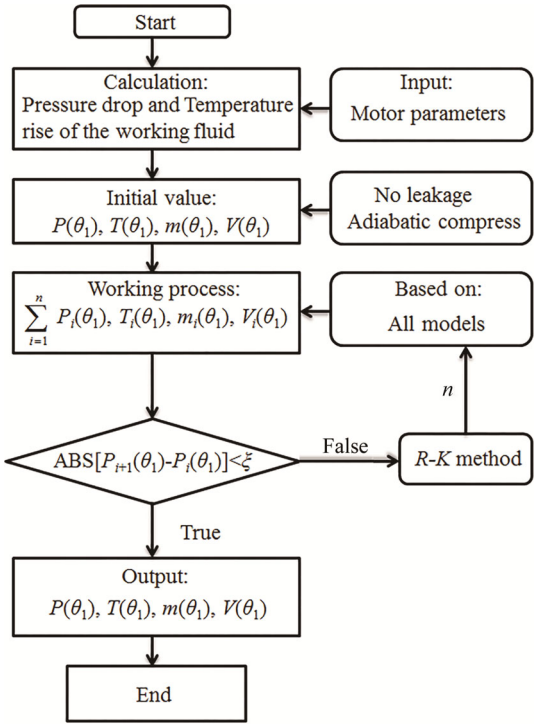


**Fig. 5** The flowchart of analysis procedure

**Table 1** Main operating and structure parameters of the single screw compressor

| Parameters | Value | Parameters | Value |
|---|---|---|---|
| Screw diameter, $d_1$ | 147 mm | Gate rotor tooth width, $b$ | 21.56 mm |
| Gate rotor diameter, $d_2$ | 147 mm | Internal volume ratio, $\lambda$ | 2.92 |
| Center distance, $A$ | 117.6 mm | Rotor length, $L_t$ | 178 mm |
| Rotation speed, $N$ | 2850 r/min | Theoretical flowing capacity, $V_d$ | 168 $m^3$/h |
| Rated power, $W$ | 45 KW | Mains frequency, $f$ | 50 Hz |
| Refrigerant | R22 | Lubricating oil | Suniso 4GSD |

The adiabatic efficiency $\eta_i$ is the ratio of the theoretical adiabatic compression power $w_{adi}$ to the shaft power $w_s$. The adiabatic efficiency is given by:

$$\eta_i = \frac{w_{adi}}{w_s} \tag{25}$$

The theoretical adiabatic compression power $w_{adi}$ is determined using the following equation:

$$w_{adi} = h_{d,ad} - h_i \tag{26}$$

where $h_{d,ad}$ is the specific enthalpy of the working fluid at the compressor outlet during the adiabatic process, and $h_i$ is the specific enthalpy of the working fluid at the inlet end.

The shaft power is the sum of the indicated power and friction power loss, and can be given by:

$$w_s = -\int_{p_i}^{p_d} v\mathrm{d}p + W_f \tag{27}$$

where $p_i$ is the inlet pressure of the compressor; $p_d$ is the outlet pressure, and $W_f$ is the friction power loss.

## 3. Experimental Study

### 3.1 Experimental system

In order to demonstrate the validity of the mathematic model, the experimental system was set up according to the gas cooling loop method, as shown in Fig. 6.

The system schematic is presented in Fig. 7, and demonstrates that the lubricating oil was separated in an oil-gas separator and subsequently injected into the compressor. The gas from the oil-gas separator was divided into two paths. One path was introduced into the mixer directly with the pressure controlled for the suction condition by the pressure controlled valve. The second path was cooled in the condenser and sub-cooler, and also injected into the mixer through the mass flow meter and thermal expansion valve. The two paths were mixed into the inlet states, which had a certain degree of superheat vapor, and the whole cycle was then completed. The outer layer of the mixer was covered with a layer of insulation cotton, such that the thermal loss of the mixer can be ignored in the calculation. The vertex flow meter was installed on the gas inlet pipe of the compressor so as to measure the volume flow rate. In addition, the experimental system also includes a water loop and a liquid injection loop.

### 3.2 Single screw compressor prototypes

Considering the leakage model, the meshing clearance between the screw groove and gate rotor tooth flank, represented by $L_2$ and $L_4$ as shown in Fig. 3, has a great influence on the SSC performance. In order to investigate the internal influence mechanism, three SSC prototypes with different clearance heights were manufactured and tested, as shown in Fig. 8, to determine the influence of the clearance on the SSC. With the exception of the clearance, each test was conducted under the same experimental conditions. Details on the clearance for the

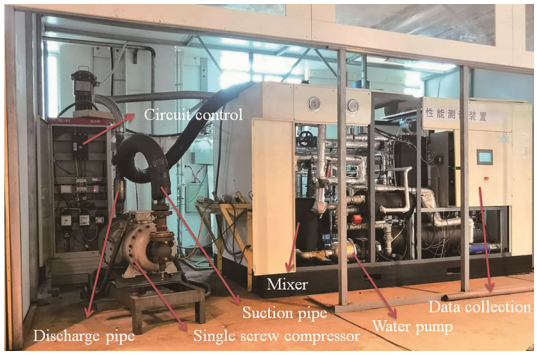


**Fig. 6** The compressor performance test system

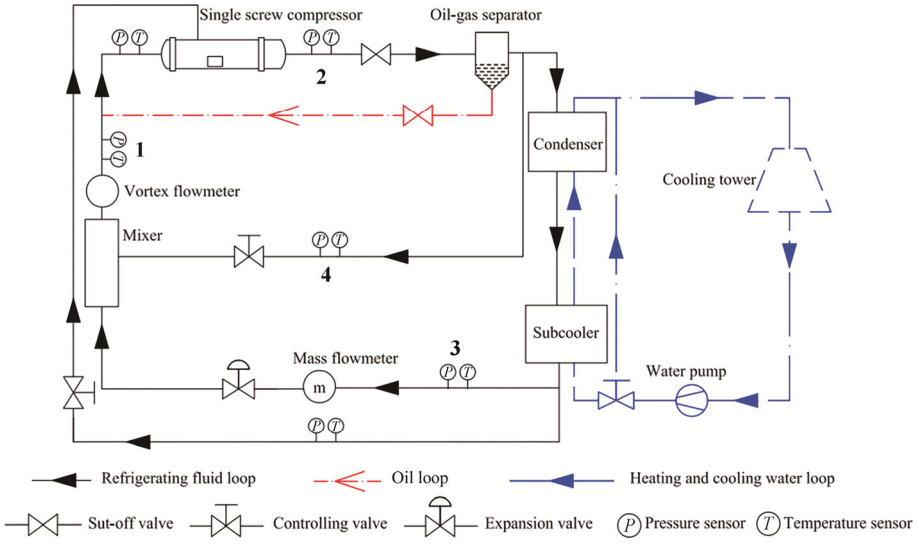


**Fig. 7** Schematic diagram of the experimental system

three prototypes are reported in Table 2. A, B and C represent the first, second and third prototypes, respectively. It is worth noting that the clearance in this study is the value under the working conditions for the refrigeration compressor. The actual assembling gaps are affected by many factors, such as thermal and forces deformations. Thus, the actual assembling clearance value should be considered in the manufacturing process according to the working conditions.

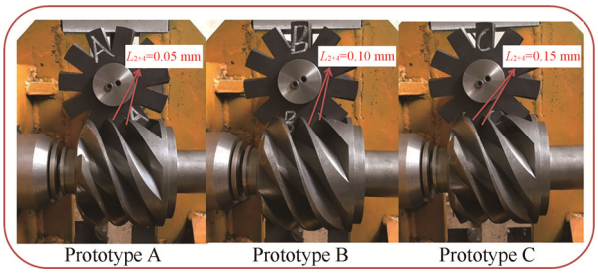


**Fig. 8** Screw rotor and gate rotor used in experimental system with different meshing clearance

**Table 2** Leakage paths clearance height values

| Leakage paths clearance height | No. A | No. B | No. C |
|---|---|---|---|
| $L_1$ | 0.02 mm | 0.02 mm | 0.02 mm |
| $L_2$=$L_4$ | 0.05 mm | 0.10 mm | 0.15 mm |
| $L_3$=$L_5$ | 0.01 mm | 0.01 mm | 0.01 mm |
| $L_6$ | 0.05 mm | 0.05 mm | 0.05 mm |
| $L_7$=$L_8$ | 0.05 mm | 0.05 mm | 0.05 mm |
| $L_9$ | 0.05 mm | 0.05 mm | 0.05 mm |

### 3.3 Experimental testing

As shown in Fig. 7, the mass flow rate of the liquid working fluid was measured using a mass flow meter with an accuracy of ±0.2%. The installation point is located behind the sub-cooler. The flow rate of the gas as it entered the compressor was measured by a vortex flow meter with an accuracy of ±1%, at the outlet of the mixer. In addition, the temperature and pressure sensors were set on the pipeline at positions 1, 2, 3 and 4 in Fig. 7. The power meter, connected to the compressor, is used to measure the input power. The accuracy and range of each measurement instrument is reported in Table 3. When the compressor works at a stable rate for more than half an hour, the experimental data were recorded. From these thermal and performance parameters, the refrigerating capacity under different working conditions can be obtained. Note that the parameters measured by the mass flow meter and vertex flow meter must be consistent through a series of calculations in order for the measured parameters to be reliable.

**Table 3** The accuracy and range of each measurement instrument

| Parameters | Range | Uncertainty |
|---|---|---|
| Temperature sensor | −30°C to 150°C | ±0.2°C |
| Pressure sensor | −0.1 to 1.5 MPa/ 0 to 4 MPa | ±1.6% |
| Mass flowmeter | 0 to 1500 kg/h | ±0.2% |
| Vertex flowmeter | 20 to 200 $m^3$/h | ±1% |
| Power meter | 20 to 60 kW | ±0.5% |

The mass and energy conservation of the mixer can be expressed using:

$$\dot{m}_1 h_1 = \dot{m}_3 h_3 + \dot{m}_4 h_4 \tag{28}$$

$$\dot{m}_1 = \dot{m}_3 + \dot{m}_4 \tag{29}$$

where $\dot{m}_1$ is the flow rate of the working fluid at the outlet of the mixer; $h_1$ is the mixer outlet specific enthalpy; $h_3$ is the specific enthalpy of the cooled liquid at the outlet of the sub-cooler; $\dot{m}_3$ is the liquid flow rate at the outlet of the subcooler; $h_4$ is the specific enthalpy of the gas at the inlet of the mixer, and $\dot{m}_4$ is the gas flow in the inlet pipe of mixer.

According to Eqs. (28) and (29), the inlet volume flow rate of the compressor can be calculated as follows:

$$V_{1\mathrm{m}} = \frac{\dot{m}_3 \left(h_3 - h_2\right)}{\rho_1 \left(h_1 - h_2\right)} \tag{30}$$

where $h_2$ is the compressor exhaust specific enthalpy, and $\rho_1$ is the mixer outlet density. Furthermore, the inlet volume flow rate of the compressor can also be measured with the vortex flow meter. In order to ensure the rationality of the experimental data, the absolute value of the difference between the calculated value $V_{1\mathrm{m}}$ and the measured value $V_{1\mathrm{c}}$ must be less than a certain threshold.

The refrigerating capacity can be calculated by:

$$\begin{cases} Q_{\mathrm{c}} = \dot{m}_1 \left(h_1 - h_{\mathrm{f2}}\right) \\ \dot{m}_1 = V_{1\mathrm{m}} \rho_1 \\ h_2 = h_4 \end{cases} \tag{31}$$

where, $h_{\mathrm{f2}}$ is the liquid specific enthalpy of the working fluid at the saturation temperature of the discharge pressure.

## 4. Results and Discussion

### 4.1 Geometrical structure parameters

Taking one groove as an example, the volume of the working chamber changes with the rotary angle of the screw rotor was analyzed based on the geometrical structure parameters shown in Fig. 9. The volume change process of the compressor includes suction, closed compress and discharge. The maximum volume of one groove is $8.16\times10^{-5}$ $m^3$ when the screw rotor rotation

angle is 0 rad. At these values, the working fluid in the working chamber will be compressed. When the screw rotor rotation angle is 1.487 rad, the gas in the compress chamber is discharged until the screw rotor rotation angle is 2.62 rad. For the test SSC, the internal volume ratio is 2.92 when the discharge process begins.

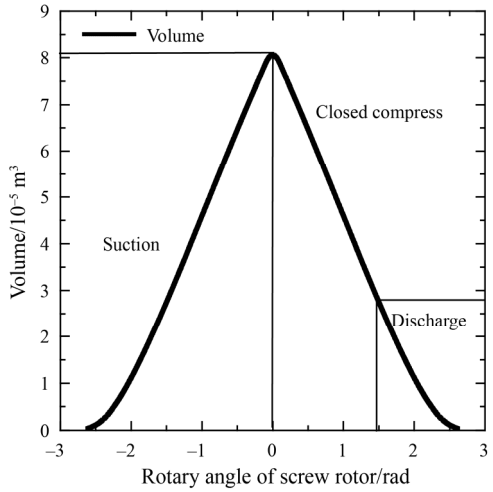


**Fig. 9** Volume of one groove changes with the screw rotor rotation angle

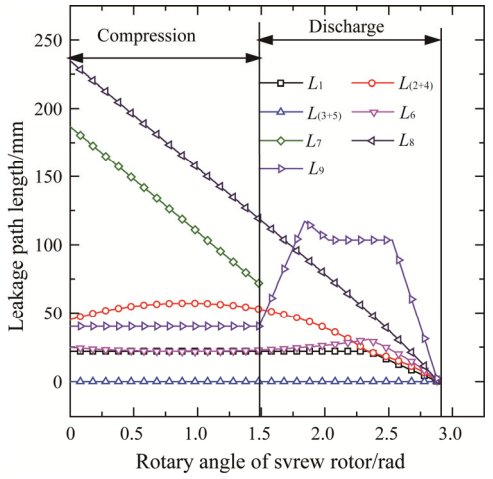


**Fig. 10** Variation in the lengths of different leakage paths with the screw rotor rotation angle

The calculation method of each leakage path length can be found in the reference [25]. Fig. 10 presents the variation in the lengths of the different leakage paths with the screw rotor rotation angle. When the screw rotor rotation angle increases, the length of $L_7$ and $L_8$ decreases, resulting in the largest leakage paths during the compression. The length of $L_{3+5}$ is invariable and small during the whole process. Because of the depth of engagement between the screw rotor and gate rotor teeth, the length of $L_{2+4}$ initially increases and subsequently decreases with the screw rotor rotation angle. The length of $L_9$ reaches a maximum when the discharge orifice joined completely during the discharge process. Thus, the remaining leakage paths contribute to the internal total leakage flow rate. When the clearance height is given, the leakage area of each leakage path can be calculated.

### 4.2 Thermodynamic performances of the working process and mathematical model validation

In order to validate the mathematical model used in this paper, prototype A was tested on the experimental system under different evaporating temperatures. The condensing temperature is set at 40°C and the superheating temperature of the inlet gas is 10°C. Before the working medium enters the compress chamber, the motor will have a large influence on the performance of the inlet gas. The decrease in pressure and increase in temperature with different evaporating temperatures during the motor segment are shown in Fig. 11. It can be seen that the pressure drop of the gas will increase, while the increment of temperature will decrease for an increasing evaporating temperature. When the evaporating temperature is 5°C, the pressure drop reaches 11.7 kPa. Moreover, for an evaporating temperature of −10°C, the temperature rise of the gas will reach 11.51°C. This can be attributed to a rise in the flow rate of the gas with increases in the evaporating temperature, resulting in an improvement in the volume efficiency because of the lower pressure ratio. Thus, the working fluid quantity used to cool the motor, as well as the power loss of motor, will also correspondingly change. In addition, the pressure drop is related to the geometric structure of the motor section, while the temperature change is dependent on the working fluid flow rate of change and the power loss of the motor, with both having opposing effects.

Fig. 12 compares $P$-$V$ values under different pressure ratios. $V_c$ is the control volume of the compressor and $V_{max}$ is the maximum value of the control volume shown in Fig. 9. The variable $t_v$ is the evaporating temperature, and $p_d/p_i$ is the pressure ratio under the working conditions for condensing pressure $p_d$ and evaporating pressure $p_i$. For pressure ratios between 2.9 and 4.3, the working process shows a clear trend towards over compression due to the fixed internal volume ratio (2.92 in this study) and the greater value of the internal pressure ratio of the compressor compared to the external pressure ratio when the discharge starts. Because the discharge orifice opens gradually, over compression is still observed for a pressure ratio value of 2.9. When $t_v$ is −10°C and the pressure ratio is 4.3, the over compression loss will suffer a corresponding decrease.

In order to demonstrate the validity of the calculation, a comparative analysis between the theoretical and experimental work was performed, as shown in Fig. 13 and Fig. 14.

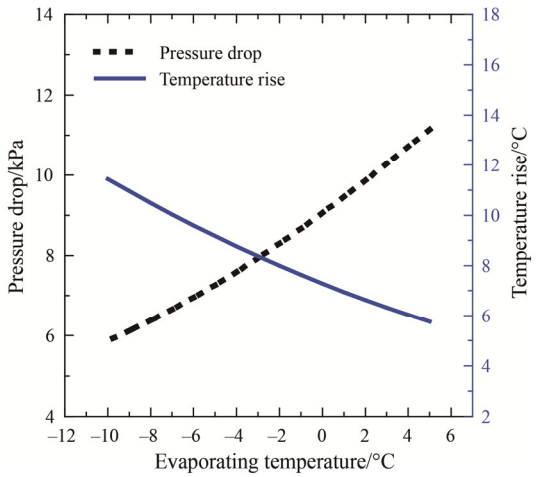


**Fig. 11** Pressure drop and temperature rise with different evaporating temperature

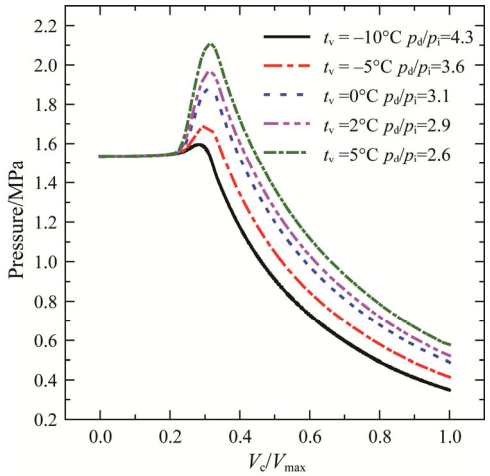


**Fig. 12** *P-V* indicator diagram comparison under different evaporating temperature

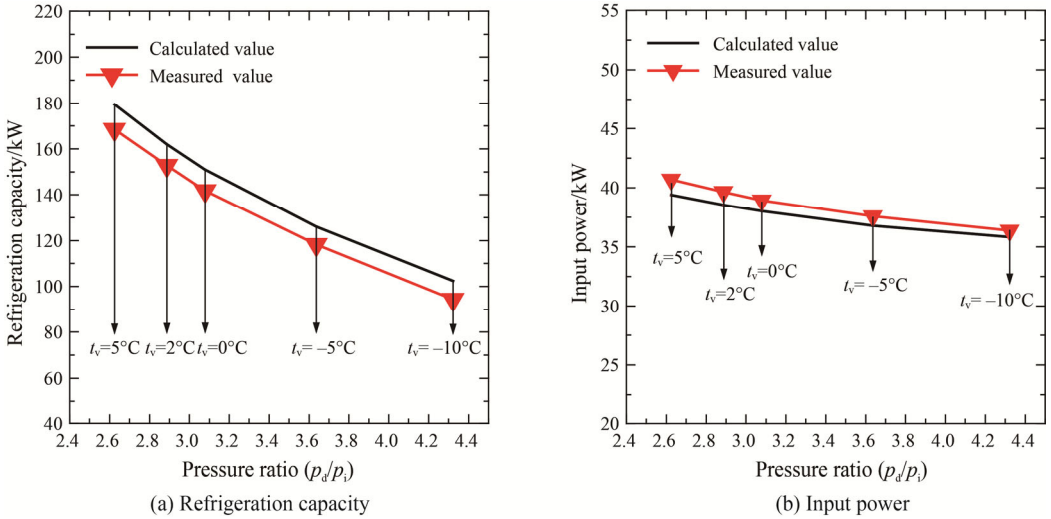


**Fig. 13** Measured and calculated results of refrigeration capacity and input power

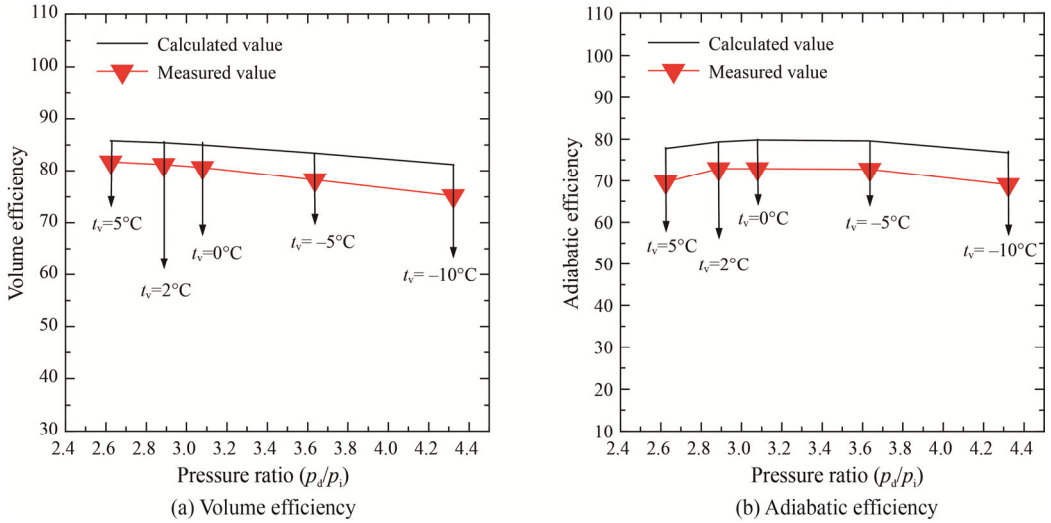


**Fig. 14** Measured and calculated results of volume efficiency and adiabatic efficiency

The refrigerating capacity and input power of prototype A under different working conditions are shown in Fig. 13(a) and (b) respectively. The calculated value of the refrigerating capacity is larger than the measured value, with a deviation of 3.98% to 7.5%. The maximum and minimum deviations between the measured and calculated input power are 3.2% and 1.5%, respectively. As shown in Fig. 14(a), the volume efficiency decreases with the increase of the pressure ratio, with a deviation of 3.6% to 7.8%. Fig. 14(b) presents the adiabatic efficiency of the compressor changes with the pressure ratio. The adiabatic efficiency increases and subsequently decreases with increases in the pressure ratio, with a deviation of 7.2% to 8.1%. This is because the internal and external pressure ratio of the compressor do not match under the test conditions, and thus the over compression loss will increase when the evaporating temperature increases, as shown in Fig. 12. The comparison of the measured and the calculated results indicates that the theoretical calculation model describing the internal working process of the compressor is reliable enough to estimate the thermodynamic performance of the compressor.

### 4.3 Theoretical analysis of thermodynamic performances of the prototypes

In order to verify the applicability of the calculated results under different meshing clearance, three prototypes were calculated and tested under the same working conditions. The condensing temperature $t_c$ is set to 40°C; the evaporating temperature $t_v$ is 5°C; the superheating temperature of inlet gas is 10°C and the pressure ratio is 3.6. According to Fig. 1, the main thermal parameters of the working fluid in three grooves (pressure, mass and temperature) are taken into account so as to better explore the internal influence mechanism of the compressor. The calculation results of prototypes A, B and C are shown in Figs. 15–17. Groove 1, groove 2 and groove 3 are adjacent compression chambers, and essentially have the same state parameters of the working medium in each groove under the same gate rotor rotation angle with a period of 60°.

Fig. 15 shows the mass in the groove changes with the screw rotor rotation angle. For a single groove, it can be seen that the mass is variable under different meshing clearances and the mass flow rate sequence is observed as follows: prototype A> prototype B >prototype C. The mass in the groove will decrease rapidly with meshing clearance increases because the amount of leakage increases at larger increments. Taking groove 2 as an example, the mass in the working chamber is still increasing during the compress process because the pressure in adjacent groove 3 is higher than the pressure in groove 2 at the same screw rotor rotation angle, as

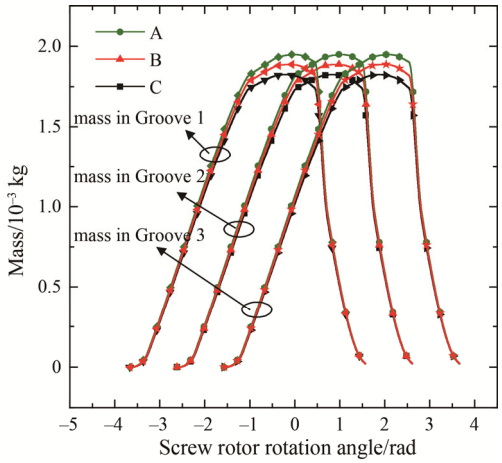


**Fig. 15** Mass in the groove changes with the screw rotor rotation angle

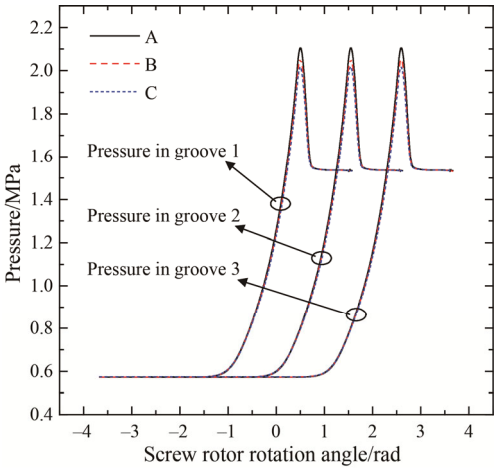


**Fig. 16** Pressure in the groove changes with the screw rotor rotation angle

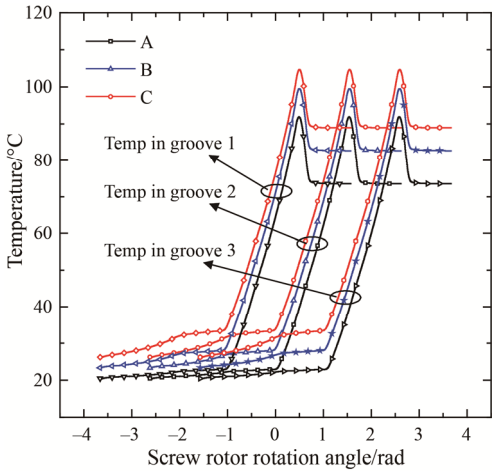


**Fig. 17** Temperature in the groove changes with the screw rotor rotation angle

shown in Fig. 16. Thus, the mass will flow from groove 3 to groove 2 through the leakage path $L_7$. When the pressure in groove 2 reaches a value that is greater than the pressure in groove 1, the mass will flow from groove 2 to groove 1 through the leakage path $L_8$. This explains why the mass in the groove will increase and subsequently decrease with the rotary angle of the screw rotor.

The values of the meshing clearance have a significant effect on temperature. The flow rate is highly variable under different meshing clearances, and the temperature rise of the working medium through the motor will also be different according to the analysis of the motor influence mechanism. Fig. 17 demonstrates how the temperature of the working medium changes with the rotary angle of the screw rotor during the whole working process. The temperature in the groove of prototype A is lower than that of prototypes B and C. The calculated discharge temperatures are 73.5°C, 82.7°C and 89.0°C for the prototypes A, B and C, respectively. Taking groove 2 as an example, the temperature will increase by 9.96°C for prototype C for screw rotor rotation angles within the range of −2.62 rad to 0 rad in one period. For prototype A, the temperature rise of the suction process will drop down to 4.90°C. The temperature variation is mainly related to the leakage through the meshing clearance and the pre-compression of the compressor. It is worth noting that higher inlet temperatures will decrease the density of the gas, thus reducing the flow rate. The higher discharge temperature will decrease the performance of the compressor significantly, and the lubricating oil may then have no effect.

### 4.4 Theoretical and experimental study on the prototypes

It can be seen that the input power of the compressor increases slowly with the decrease of the meshing clearance height, while the calculated refrigerating capacity increases rapidly. Based on the experimental results, when the clearance value decreases, the volume ratio will also improve significantly, from 62.8% to 82.1%. For the compressor of prototype C, the discharge temperature is higher than prototypes A and B, reaching 89.0°C, and the deviation between experimental and calculated results is 0.33%. It can be seen that the experimental results are in good agreement with the calculated results.

### 4.5 Theoretical analysis under different meshing clearances

The slide valve control mechanical device of the SSC can be used to adjust the internal pressure ratio so as to meet the requirements of the actual operating conditions, thus minimizing the over or under compression loss. Based on this condition, the volume efficiency and adiabatic efficiency under different working conditions are calculated in this paper in order to analyze the performance of the single screw compressor under different meshing clearances. Fig. 18 shows the variation in the volume efficiency with the meshing clearance height. Here, $t_v$ is the evaporating temperature and $t_c$ is the condensing temperature (40°C is used here). The pressure ratio decreases from 5.2 to 2.6 with the increase of evaporating temperature. The volume efficiency decreases when the meshing clearance height increases, and the drop at high pressure ratios is greater than the drop at low pressure ratios.

From Fig. 18(a), it can be seen that for a pressure ratio of 5.2, the volume efficiency decreases from 86.7% to 63.9% when the meshing clearance height increases from 0.01 mm to 0.15 mm. Moreover, when the pressure ratio value is 2.6, the volume efficiency will decrease from 92.5% to 79.8%. This demonstrates that the volume efficiency will drop rapidly under larger pressure ratios and increases in the meshing clearance. The decrease in volumetric efficiency can be attributed to the decrease in the mass flow rate, as the internal leakage rate increases when the meshing clearance height increases. As discussed for Fig. 15, the mass in the working chamber is reduced when the meshing clearance height increases. Moreover, the volumetric efficiency decreases with increases in the pressure ratio at a certain meshing clearance. This is because the leakage flow rate will increase when the pressure ratio increases.

**Table 4** Comparison between the experimental and calculated results from this section. $P_s$ is the input power; $Q_c$ is the refrigerating capacity; $\eta_v$ is the volume efficiency; $\eta_i$ is the adiabatic efficiency and $T_d$ is the discharge temperature.

| State parameters | No. A | | | No. B | | | No. C | | |
|---|---|---|---|---|---|---|---|---|---|
| | Measured | Calculated | Error | Measured | Calculated | Error | Measured | Calculated | Error |
| $P_s$ | 40.7 kW | 39.4 kW | 3.19% | 39.2 kW | 38.6 kW | 1.55% | 40.0 kW | 37.8 kW | 5.50% |
| $Q_c$ | 168.5 kW | 175.5 kW | 3.98% | 145.7 kW | 156.3 kW | 6.78% | 120.0 kW | 127.7 kW | 6.03% |
| $\eta_v$ | 82.1% | 85.2% | 3.64% | 73.2% | 76.8% | 4.69% | 62.2% | 67.6% | 7.98% |
| $\eta_i$ | 72.1% | 77.7% | 7.20% | 66.8% | 71.0% | 5.92% | 55.3% | 64.7% | 9.40% |
| $T_d$ | 70.0°C | 73.5°C | 4.75% | 83.6°C | 82.7°C | 1.03% | 88.7°C | 89.0°C | 0.33% |

Fig. 19 presents the adiabatic efficiency changes with the meshing clearance height under different working conditions. Initially, the adiabatic efficiency decreases slowly, and then rapidly with the increase of the meshing clearance height. More specifically, when the pressure ratio is 5.2, the adiabatic efficiency decreases from 75.4% to 62.2%, with meshing clearance height values from 0.01 mm to 0.15 mm. This is because at a larger meshing clearance height, the mass flow leakage rate out of the working chamber is greater than that leaked into the working chamber, resulting in a lower mass flow rate and a higher inlet temperature, as discussed for Fig. 15 and Fig. 17. It can also be observed that the adiabatic efficiency decreases with pressure ratio increases, with this decrease exhibiting an accelerating trend. This decrease in adiabatic efficiency is observed because the mass flow rate will fall due to the higher pressure ratio and larger leakage rate. When the evaporating temperature is constant at −5°C, the adiabatic efficiency decreases with condensing temperature increases at certain meshing clearance heights, as both the pressure ratio and the leakage rate will increase with condensing temperature rises.

Figs. 18 and 19 show that the volume efficiency attains lower values when the meshing clearance height is larger than 0.08 mm, and that the decrement of the adiabatic efficiency will also increase rapidly. For meshing clearance heights within the range of 0.01 to 0.08 mm, the volume efficiency will be higher than 80% and the adiabatic efficiency will reach 70% or more under normal operating conditions. Based on the analysis above, both the volume efficiency and adiabatic efficiency will decrease with meshing clearance height increases, and the decrement will be greater at larger

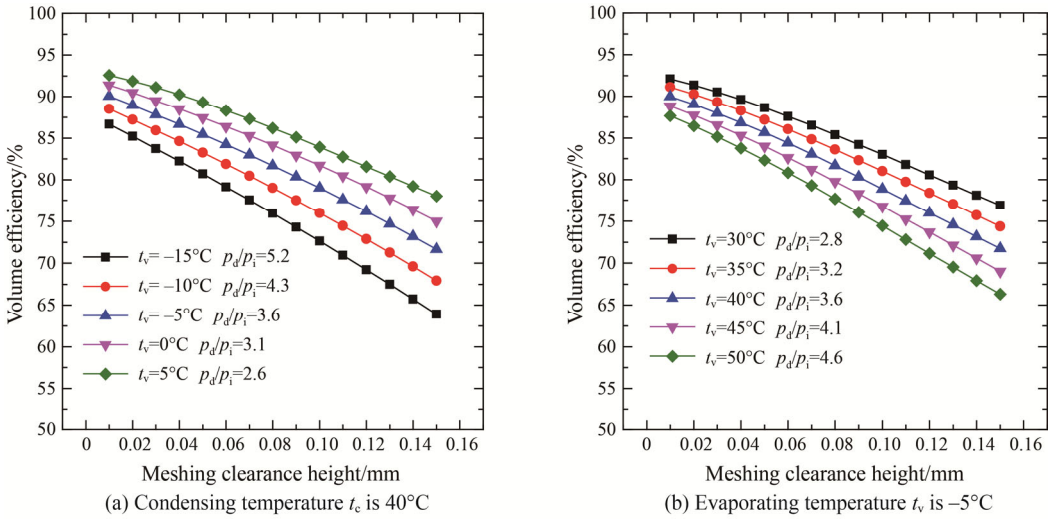


(a) Condensing temperature $t_c$ is 40°C (b) Evaporating temperature $t_v$ is –5°C

**Fig. 18** Variation in volume efficiency with the meshing clearance height value

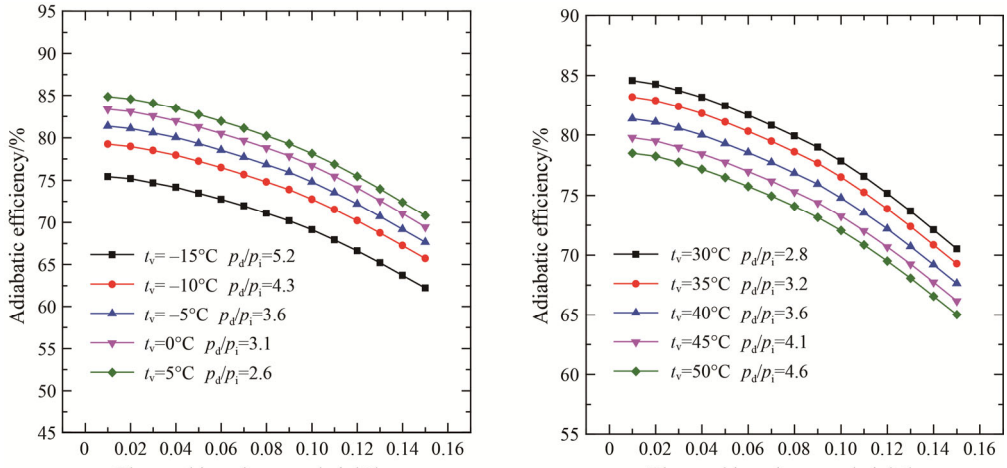


(a) Condensing temperature $t_c$ is 40°C (b) Evaporating temperature $t_v$ is –5°C

**Fig. 19** Variation in adiabatic efficiency with the meshing clearance height

meshing clearance heights. Considering the limitation of actual manu- facturing conditions, meshing clearance heights under real-world working conditions between 0.01 mm and 0.08 mm are suggested.

### 4.6 Uncertainty analysis

It is necessary to verify the accuracy of the experimental results. The methods of standard error analysis were used to evaluate the uncertainties of the calculated results. The measurement errors include systematic and random errors. Systematic errors are related to the measuring equipment. And the random errors are related to the data plots after the same measurements are repeated. In this paper, the variables involved are pressure, power, temperature and the flow rate. The error transfer relationship can be calculated using the following equation:

$$\delta y=\sqrt{\left(\frac{\partial y}{\partial x_1}\delta x_1\right)^2+\left(\frac{\partial y}{\partial x_2}\delta x_2\right)^2+\cdots\cdots+\left(\frac{\partial y}{\partial x_n}\delta x_n\right)^2} \quad (32)$$

Specifically, the desired result is a well-behaved function $y(x_1,x_2,\ldots x_n)$ of the direct physical variables $(x_1,x_2,\ldots x_n)$ that have uncertainties $(\delta x_1, \delta x_2,\ldots \delta x_n)$. The total relative accuracy of the test results can be obtained using:

$$\delta_y=\frac{\Delta y}{y}\times 100\% \quad (33)$$

According to the accuracy of each measurement instrument shown in Table 3, the total relative accuracy of the refrigerating capacity is 2.58%.

## 5. Conclusions

In this paper, a mathematical model considering leakage, heat transfer, the motor of the compressor and the lubricating oil, was developed in order to analyze the working process of the SSC under different meshing clearances and working conditions. Changes with varying screw rotation angles of the main state parameters, including the temperature, mass and pressure, of the working medium in the working chamber were calculated. Three SSC prototypes with different clearance height controls were manufactured and tested on the experimental system. Based on the analysis, the following conclusions are obtained:

(1) The motor of the SSC will have a noticeable influence on the thermo-physical properties of the working fluid. The pressure drop of the working medium will increase and the increment of temperature will decrease with evaporating temperature increases due to the increase of the mass flow rate.

(2) The calculation results of prototype A under different test conditions are in agreement with the experimental results. The maximum deviation of the volume efficiency and adiabatic efficiency are 8.8% and 8.1%, respectively. The results show that the calculation model is reliable enough to estimate the thermodynamic performance of the single screw compressor.

(3) Compared with prototypes B and C, prototype A demonstrated the best performance. Prototype A has the highest volume and adiabatic efficiency, at 82.1% and 72.1% respectively, based on the experimental results. The influence of the meshing clearance height on the performance of the compressor was significant, particularly for the discharge and inlet temperature. The higher inlet temperature will decrease the density of the gas and the flow rate will subsequently fall. The performance of prototype C is poor because of the larger meshing clearance height, with a 88.7°C discharge temperature and a 55.3% adiabatic efficiency.

(4) When the meshing clearance height rises, the volume efficiency and adiabatic efficiency will decrease rapidly. The mainly reason is that the larger pressure ratio and leakage leads to a lower efficiency. Considering the working performance under normal operating conditions, the limitation of actual manufacturing conditions and manufacturing costs, meshing clearance heights under real-world working conditions from 0.01 mm to 0.08 mm are suggested. It is worth noting that the actual assembling clearance value should be considered in the design and production processes according to the working conditions because of the effect of thermal and force deformations.

## Acknowledgement

The authors are grateful for the financial support provided by the National Key R&D Program of China (NO. 2016YFC0700403), Beijing Municipal Natural Science Foundation (NO. 3181001). Project supported by Beijing Chaoyang District Postdoctoral Research Foundation (NO. 2018ZZ-01-28).

## References

[1] Yue S.Y., Wang Y.G., Wang H.T., Design and optimization of tandem arranged cascade in a transonic compressor. Journal of Thermal Science, 2018, 27: 349–358.

[2] Wang S.H., Single screw refrigeration compressor. Chemical and General Machinery, 1978, 07: 50–52. (in Chinese)

[3] Li Y., Xie G.N., et al., Performance study on a single-screw compressor for a portable natural gas liquefaction process. Energy, 2018, 148: 1032–1045.

[4] Zimmern B., Worm rotary compressors with liquid joints. 1965, U.S. Patent No. 3180565.

[5] Wu H., Peng X., Xing Z., et al., Experimental study on p-V indicator diagrams of twin-screw refrigeration compressor with economizer. Applied Thermal Engineering, 2004, 24: 1491–1500.
[6] Wang W., Wu Y.T., Ma C.F., et al., Experimental study on the performance of single screw expanders by gap adjustment. Energy, 2013, 62: 379–384.
[7] Zimmern B., Rotary inter-engaging worm and worm wheel with specific tooth shape. 1976, U.S. Patent No. 3932077.
[8] Huang R., Li T., et al., An optimization of the star-wheel profile in a single screw compressor. Institution of Mechanical Engineers Part A: Journal of Power and Energy, 2015, 229(2): 139–150.
[9] Wu W.F., Feng Q.K., A multicolumn envelope meshing pair for single screw compressors. Journal of Mechanical Design, 2009, 131, paper No. 074505.
[10] Wang Z.L., Wang H., et al., Optimization study on multicolumn envelope meshing pair of single screw compressor based on leakage characteristics. International Journal of Refrigeration, 2018, 92: 113–124.
[11] Li T., Liu Z., et al., Research of the hydrodynamic lubrication characteristics of different meshing pair profiles in water-flooded single screw compressors. Institution of Mechanical Engineers Part A: Journal of Power and Energy, 2016, 230(3): 247–259.
[12] Nikola S., Smith I.K., et al., Review of Mathematical Models in Performance Calculation of Screw Compressors. International Journal of Fluid Machinery and systems, 2011, 4(2): 200–217.
[13] Fujiwara M., Kasuya K., Matsunaga T., Watanabe M. Computer modeling for performance analysis of rotary screw compressor. International Compressor Engineering Conference at Purdue, 1984, paper No. 503.
[14] Fukazawa Y., Ozawa U., Small screw compressors for automobile air conditioning systems. International Compressor Engineering Conference at Purdue, 1980, paper no. 351.
[15] Sangfors B., Computer simulation of the oil injected twin screw compressor. International Compressor Engineering Conference at Purdue, 1984, paper No. 502.
[16] Zimmern B., Design and operating characteristics of the Zimmern single screw compressor. International Compressor Engineering Conference, 1972, paper No. 16.
[17] Moore J., Computer modeling of single-screw oil flooded refrigerant compressors. International Compressor Engineering Conference, 1984, paper No. 506.
[18] Li H.Q., Jin L.W., Design optimization of an oil-flooded refrigeration single screw compressor. International Compressor Engineering Conference, 2004, paper No. 1715.
[19] Yang J.L., Zhang C., Zhang Z.T., et al., Study on mechanical vapor recompression system with wet compression single screw compressor. Applied Thermal Engineering, 2016, 103: 205–211.
[20] Wang Z.L., Wang Z.B., et al., Research of thermal dynamic characteristics for variable load single screw refrigeration compressor with different capacity control mechanism. Applied Thermal Engineering, 2017, 110: 1172–1182.
[21] Wang Z.L., Shen Y.F., et al., Theoretical research and optimization analysis for the injection process of the single screw refrigeration compressor. International Journal of Refrigeration, 2018, 88: 91–101.
[22] Zhao B., Yang M.S., et al., Heat transfer analysis of single screw compressor under oil atomization based on fuzzy random wavelet finite element method. International Communications in Heat and Mass Transfer, 2016, 77: 43–48.
[23] Smith S.L., Mimeche C., Void fractions in two-phase flow: A correlation based upon an Equal velocity head model. Instrumentation of Mechanical engineers, 1969, 184(36): 647–664.
[24] Shen L.L., Wang W., Wu Y.T., et al., Theoretical and experimental analyses of the internal leakage in single-screw expanders. International Journal of Refrigeration, 2018, 86: 273–281.
[25] Tang H., Wu H.G., Wang X.L., et al., Performance study of a twin-screw expander used in a geothermal organic Rankine cycle power generator. Energy, 2015, 90: 631–642.
[26] Wu H.G., Li J.F, Xing Z.W., et al., Theoretical and experimental research on the working process of screw refrigeration compressor under superfeed condition. International Journal of Refrigeration, 2007, 30: 1329–1335.
[27] Shen L.L., Wang W., Wu Y.T., et al., A study of clearance height on the performance of single screw expanders in small-scale organic Rankine cycles. Energy, 2018, 153: 45–55.
[28] Wu Y.T., Zhi R.P., Wang W., et al., mathematical modeling of torque for single screw expanders. Journal of Mechanical Science and Technology, 2017, 31(1): 429–436.
[29] Zhou L., Thermal elastic deformation and the dynamic meshing characteristics research of the meshing pair in single screw compressor. PhD Thesis. Xi'an Jiaotong University; 1999. (in Chinese)
[30] White F.M., Fluid mechanics. New York: McGraw-Hill, 2010.
[31] Yang L., Dai W.J., et al., Electric machine design theory and practice, Tsinghua University Press, Beijing, 2013, pp. 53–77. (in Chinese)
[32] Martin J.J., Hou Y.C., Development of an equation of state for gases. American Institute of Chemical Engineer Journal, 1955, 2(1): 142–151.